

# International Journal of Applied Mathematics in Control Engineering

Journal homepage: <http://www.ijamce.com>

## Zero-Watermarking Algorithm Based on Image Normalization and 2D-LPEWT

Lvmuzhi Li<sup>a</sup>, Kunjie Cai<sup>a</sup>, Shuai Li<sup>a</sup>, Jincai Chang<sup>a,b\*</sup><sup>a</sup> College of Science, North China University of Science and Technology, Hebei Tangshan 063200, China<sup>b</sup> Hebei Key Laboratory of Science and Application, Hebei Tangshan 063210, China

### ARTICLE INFO

Article history:

Received 5 July 2022

Accepted 10 October 2022

Available online 15 October 2022

Keywords:

Image normalization

2D-LPEWT

Schur decomposition

Zero-watermarking

Robustness

### ABSTRACT

In order to improve the robustness of zero-watermarking, this paper proposes a robust zero-watermarking algorithm based on Two-Dimensional Littlewood-Paley empirical wavelet transform (2D-LPEWT) and Schur decomposition. The algorithm first normalizes the original image, then corrects and removes the black edges, and then performs 2D-LPEWT; selects low-frequency subbands for chunking Schur decomposition, extracts the largest element in the diagonal element of the triangular matrix on the decomposed chunk, and constructs the transition matrix; compares the average value of this matrix with each element value to generate the characteristic binary matrix; and then after the Arnold transform, the watermark information is encrypted with the generated eigenbinary matrix and then the zero-watermarking is obtained by the dissimilarity operation; finally, the registration is completed at the third-party Intellectual Property Rights (IPR). The experiments show that the robustness against non-geometric and geometric attacks is improved compared with the existing robust zero-watermarking based on wavelet transform.

Published by YX.Union. All rights reserved.

## 1. Introduction

The threshold for digital content creation has gradually been lowered, and digital content such as online literature, pictures, audio and video has exploded and the digital content market has seen rapid prosperity. The accompanying digital copyright infringement is also increasing day by day, and disputes in online copyright lawsuits are frequent.

In order to solve the contradiction between robustness and transparency of digital watermarking, Wen et al. proposed the concept of zero-watermarking, which plays a protective role for the integrity of carrier information since the zero-watermarking algorithm does not require embedding copyright information into the carrier information. Therefore, in recent years, zero-watermarking algorithms have received a lot of attention in the field of copyright protection.

In 2011 Shobana et al. proposed a novel watermarking algorithm using complex wavelet transform and Singular Value Decomposition (SVD). The SVD based image produces zero-watermarking sequence using zero-watermark algorithm. Prathap et al. used Contourlet transform to extract the low frequency information of carrier images and constructed feature information

by Principal Component Analysis (PCA) to construct a zero-watermarking. Waleed et al. proposed a genetic algorithm based robust zero-watermarking technique for secret watermark sharing. Implemented in Discrete Cosine Transform (DCT) of grayscale images, genetic algorithm based zero-watermarking is used to select the optimal location for extracting image robust features. In 2018, Yang et al. proposed a strongly robust zero-watermarking algorithm based on Non-Subsampled Contourlet Transform (NSCT) and image normalization. In the proposed scheme, the overlay image is mapped to the geometrically invariant space by using invariant moment-based image normalization technique. Then, the effective part of the normalized image is extracted using the square of the unit circle and NSCT is performed, and the low-frequency tethering is decomposed by chunking singular values to generate a zero-watermarking based on the highest bit odd of the maximum singular value of each chunk. Gao and Jiang generate feature vectors using Bessel-Fourier moments of the normalized image and generate zero-watermarking images; the algorithm uses the rotational invariance of Bessel-Fourier moments to resist image rotation and image offset operations. As a technical branch of digital watermarking, zero-watermarking is a good solution to the imbalance between transparency and robustness of traditional watermarking techniques.

\* Corresponding author.

E-mail addresses: [jincal@ncst.edu.cn](mailto:jincal@ncst.edu.cn) (J. Chang)

Doi:

## 2. Preliminary

### 2.1 Arnold Transform

Arnold transform is a classical encryption algorithm based on image pixel point dislocation. Its principle is to achieve the effect of image encryption by transforming and disrupting the pixel points in an image to eliminate the correlation between adjacent pixels of the image using the following equation, as shown in Equation (1).

$$\begin{bmatrix} x' \\ y' \end{bmatrix} = \begin{bmatrix} 1 & 1 \\ 1 & 2 \end{bmatrix} \begin{bmatrix} x \\ y \end{bmatrix} \text{mod}(N) \quad (1)$$

where  $(x, y)$  are the original coordinates of the pixel points and  $(x', y')$  are the coordinates of the pixel points after the pixel points are scrambled. In order to have an inverse transformation and to limit the location of the updated pixel points to the length and width of the original image,  $N$  is generally taken as the length or width of the image with the same aspect.

### 2.2 Empirical Wavelet Transform (EWT) and Empirical Modal Decomposition (EMD)

In 1998, Huang et al. proposed the concept of Empirical Mode Decomposition (EMD), which automatically decomposes a signal into a finite number of Intrinsic Mode Function (IMF) components based on signal characteristics. However, there are two main problems in applying the empirical mode decomposition method. First, it lacks a mathematical theory. Second, it does not guarantee that the different input images will fit each other.

In 2013 Gilles proposed the Empirical Wavelet Transform (EWT), which is a non-smooth signal processing method. The method is able to identify the location of feature information in the Fourier spectrum of a signal using a wavelet filter bank with tight support characteristics, adaptively extracting to the different frequency components of the signal. The empirical wavelet transform consists of two main steps: firstly, the Fourier spectrum of the original signal is segmented; then, the empirical wavelet function  $\Psi_n(\omega)$  and the empirical scale function  $\varphi_n(\omega)$  are constructed and the detail and approximation coefficients are calculated. The proposed empirical wavelet transform solves the two main problems of EMD.

### 2.3 Two-Dimensional Empirical Wavelet Transform (2D EWT)

The extension of the 1D EWT to 2D images by the tensor product method was considered at the same time as Gilles proposed the 1D empirical wavelet transform, just like the usual 2D discrete wavelet transform. The idea was to use the 1D EWT on the rows and columns separately.

The 2D Littlewood-Paley wavelet transform corresponds to a filtered image in which a 2D wavelet (centred at the origin) is defined in the Fourier domain on a toroidal support. The inner and outer radius of these supports are fixed on a binary decomposition of the Fourier plane. This is then easily applied to an image whose Fourier energy is spread over two consecutive support domains, allowing separation of this information after wavelet filtering. Empirical methods are applied in this algorithm to detect the radius of each ring, and the best way to perform this detection is to consider the Fourier plane in a polar coordinate representation, finding such a boundary equivalent to using the frequency  $|\omega|$ . References have constructed an operator  $F_p(f)(\theta, |\omega|)$  to deal with

the Fast Fourier Transform (FFT) problem of pseudo-poles. For each angle  $\theta$ , there is a one-dimensional Fourier spectrum corresponding to it. The advantage of this procedure is that it considers the Fourier plane in a non-polar representation.

However, for tensor transforms, if each Fourier boundary detection is performed independently, discontinuities will be introduced in the output components. Discontinuities in output components in tensor transformations can be prevented by computing the average spectrum. where  $\theta$  is averaged, which is

$$F(|\omega|) = \frac{1}{N_\theta} \sum_{i=0}^{N_\theta-1} F_p(f)(\theta_i, |\omega|), \text{ where } N_\theta \text{ is the number of}$$

discrete angles. Then perform Fourier boundary detection on

$$F(|\omega|) \text{ to get the spectral radius } B^{\text{ELP}} = \{\phi_1(x), \{\psi_n(x)\}_{n=1}^{N-1}\},$$

where the empirical scaling function  $F_2(\phi_1)(\omega)$  and the empirical wavelet function  $F_2(\psi_n)(\omega)$  are:

$$F_2(\phi_1)(\omega) = \begin{cases} 1 & |\omega| \leq (1-\gamma)\omega^1 \\ \cos[\frac{\pi}{2} \beta(\frac{1}{2\gamma\omega^1} (|\omega| - (1-\gamma)\omega^1))] & (1-\gamma)\omega^1 \leq |\omega| \leq (1+\gamma)\omega^1 \\ 0 & \text{else} \end{cases} \quad (2)$$

$$F_2(\psi_1)(\omega) = \begin{cases} 1 & (1+\gamma)\omega^n \leq |\omega| \leq (1-\gamma)\omega^{n+1} \\ \cos[\frac{\pi}{2} \beta(\frac{1}{2\gamma\omega^{n+1}} (|\omega| - (1-\gamma)\omega^{n+1}))] & (1-\gamma)\omega^{n+1} \leq |\omega| \leq (1+\gamma)\omega^{n+1} \\ \sin[\frac{\pi}{2} \beta(\frac{1}{2\gamma\omega^n} (|\omega| - (1-\gamma)\omega^n))] & (1-\gamma)\omega^n \leq |\omega| \leq (1+\gamma)\omega^n \\ 0 & \text{else} \end{cases} \quad (3)$$

$$F_2(\psi_{N-1})(\omega) = \begin{cases} 1 & (1+\gamma)\omega^{N-1} \leq |\omega| \\ \sin[\frac{\pi}{2} \beta(\frac{1}{2\gamma\omega^{N-1}} (|\omega| - (1-\gamma)\omega^{N-1}))] & (1-\gamma)\omega^{N-1} \leq |\omega| \leq (1+\gamma)\omega^{N-1} \\ 0 & \text{else} \end{cases} \quad (4)$$

When an image  $f$  is input, the approximation coefficient

$$W_f^{\text{ELP}}(0, x) \text{ and the detail coefficient } W_f^{\text{ELP}}(n, x) \text{ after the 2D}$$

empirical Littlewood-Paley wavelet transform are

$$W_f^{\text{ELP}}(0, x) = F_2^*(F_2(f)(\omega) \overline{F_2(\phi_1)(\omega)}) \quad (5)$$

$$W_f^{\text{ELP}}(n, x) = F_2^*(F_2(f)(\omega) \overline{F_2(\psi_n)(\omega)}) \quad (6)$$

The original input image  $f(x)$  can be obtained by the following inverse transformation formula(7):

$$f(x) = F_2^*(F_2(W_f^{\text{ELP}})(0, \omega) \overline{F_2(\phi_1)(\omega)} + \sum_{n=1}^{N-1} F_2(W_f^{\text{ELP}})(n, \omega) \overline{F_2(\psi_n)(\omega)}) \quad (7)$$

The flow of 2D Littlewood-Paley empirical wavelet processing

image is shown in Figure 1:

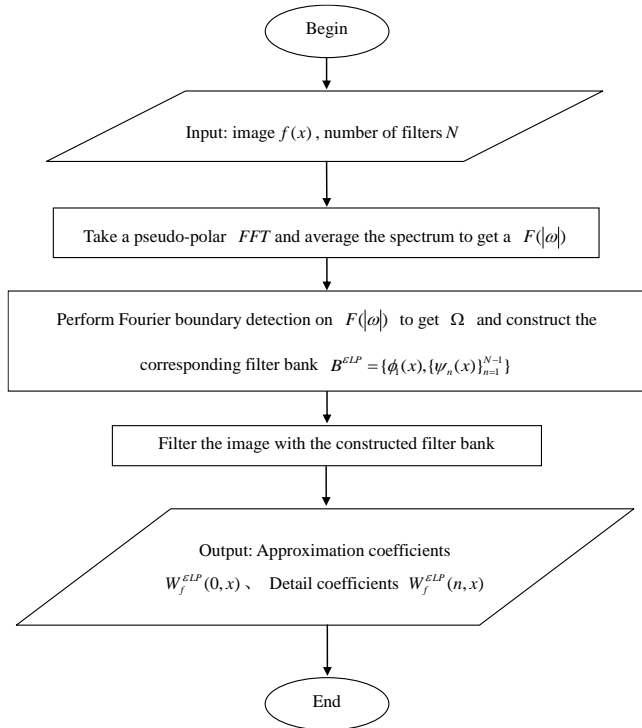


Fig. 1. 2D Littlewood-Paley empirical wavelet processing image flow chart

As shown in Figure 2, it is the result of processing the grayscale Barbara image through the 2D Littlewood-Paley empirical wavelet transform. The number of defined filters is 6, the upper left corner is the approximated component after transformation, and the rest are transformed after the detail component.

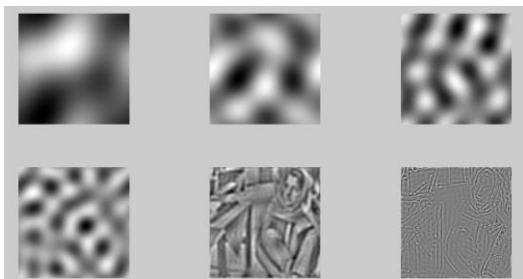


Fig. 2. Example of 2D Littlewood-Paley empirical wavelet transform results

Compared with the classical 2D discrete wavelet transform, the two-dimensional empirical wavelet transform has the advantage that the wavelet function and the scale function can be adaptively generated according to the characteristics of the image. The classical wavelet transform uses a fixed wavelet function and scale function for image decomposition, which has nothing to do with image characteristics.

At present, the 2D empirical wavelet transform and its improved algorithms have been widely used in signal noise reduction, image noise reduction, image fusion, digital watermarking, privacy protection and other fields.

### 2.4 Schur Decomposition

Schur decomposition is a basic matrix decomposition method. Its function is to directly decompose the image matrix into a unitary matrix  $U$  and an upper triangular matrix  $T$  multiplied, that is,  $A = UTU^H$ . In SVD, Schur decomposition is one of the steps,

which not only retains the good performance of SVD, but also reduces the computation time by two-thirds of the time required by the original SVD. In addition, Schur decomposition also has the characteristics of rotation invariance and robustness, and is widely used in the field of digital watermarking.

### 2.5 Image Moment Normalization

The essence of image moment normalization is to use the invariance of the moment to obtain the image in a special affine transformation to obtain the standard image. Each digital image has its own unique image moment, Define a digital image  $f(x, y)$ , the definition of its  $(p + q)$  moment:

$$m_{p,q} = \sum_{x=0}^{M-1} \sum_{y=0}^{N-1} x^p y^q f(x, y)$$

Where  $n, m$  are the height and width of the digital image, and then the definition of the central moment can be obtained:

$$\mu_{p,q} = \sum_{x=0}^{M-1} \sum_{y=0}^{N-1} (x - \bar{x})^p (y - \bar{y})^q f(x, y) \quad \text{where } \bar{x} = \frac{m_{1,0}}{m_{0,0}}, \bar{y} = \frac{m_{0,1}}{m_{0,0}}$$

$(\bar{x}, \bar{y})$  are the centroid of the digital image. Thus, the covariance matrix of the digital image  $f$  can be obtained:

$$M = \frac{1}{m_{0,0}} \begin{pmatrix} \mu_{2,0} & \mu_{1,1} \\ \mu_{1,1} & \mu_{0,2} \end{pmatrix}, \quad \lambda_1, \lambda_2 \text{ are the eigenvalues of } M, \text{ and}$$

finally the image is normalized to the form:

$$\begin{bmatrix} x' \\ y' \end{bmatrix} = \begin{bmatrix} \cos \theta & \sin \theta \\ -\sin \theta & \cos \theta \end{bmatrix} \begin{bmatrix} \frac{c}{\sqrt{\lambda_1}} & 0 \\ 0 & \frac{c}{\sqrt{\lambda_2}} \end{bmatrix} \begin{bmatrix} x - \bar{x} \\ y - \bar{y} \end{bmatrix} \quad (8)$$

The image moment normalization method realizes translation normalization, rotation normalization and scale normalization, and has good translation invariance, rotation invariance and scale invariance.

The image normalization process to form a standard image process is shown in Figure 3:

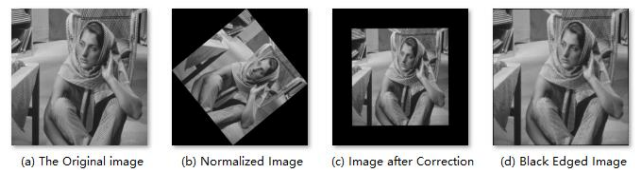


Fig. 3. The original image is normalized and formed into a standard image schematic diagram

## 3. Zero-watermarking algorithm

### 3.1 Zero-watermarking generation process

Step1: The grayscale image  $H$  of size  $M \times M$  is selected as the carrier image, and the binary image  $W$  of size  $N \times N$  is the watermark image. The watermark image is encrypted using Arnold scrambling algorithm to obtain the encrypted watermark  $W'$ .

Step2: Perform moment normalization on the image  $H$  to obtain the standard image  $B$ , and after correcting the standard image  $B$ , remove the black edge, and extract the effective image  $D$ .

Step3: Perform 2D-LPEWT on image  $D$ , and divide the

transformed image low-frequency subband  $E$  into non-overlapping sub-blocks of size  $8 \times 8$ , denoted as  $E_{i,j}(i, j = 1, 2, \dots, M/8)$ .

Step4: Matrix Schur decomposition for each subblock.

$$[Q_{i,j}, S_{i,j}] = schur(E_{i,j}) \quad (9)$$

$Q_{i,j}$  is the unitary matrix decomposed by each sub-block  $E_{i,j}$ , and  $S_{i,j}$  is the upper triangular matrix.

Step5: Take the maximum value of each sub-block  $E_{i,j}$  and denote it as  $E_{(i,j)max}$ , and use  $E_{(i,j)max}$  to construct a transition feature matrix  $F$  of size  $(M/8) \times (M/8)$ , that is,

$F_{(i,j)} = E_{(i,j)max}$ , where  $(i, j = 1, 2, \dots, M/8)$ , and calculate the sum of the elements in the transition matrix  $F$  to obtain the mean value and denote it as  $F_{mean}$ .

Step6: Generate a binary feature matrix, compare each element in the transition matrix  $F$  with its mean  $F_{mean}$  by formula(10), and obtain  $I_{i,j}$ .

$$I_{(i,j)} = \begin{cases} 1, & F_{(i,j)} > F_{mean} \\ 0, & else \end{cases} \quad (10)$$

Step7: Construct the zero-watermarking  $Z$ , and perform the XOR on the  $W'$  of the scrambled and encrypted watermark image and the generated binary feature matrix  $I$ .

$$Z = W' \otimes I \quad (11)$$

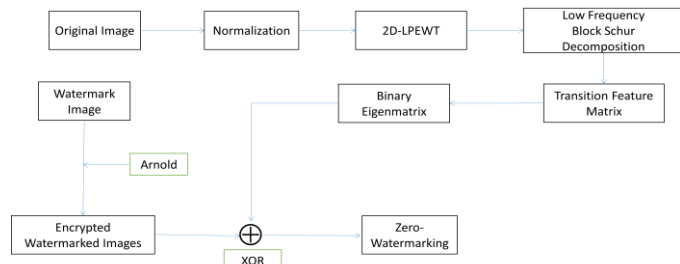


Fig. 4. Zero-watermarking generation algorithm

### 3.2 Zero-watermarking extraction process

Step1: Perform moment normalization on the image  $H'$  to obtain the standard image  $B'$ , and after correcting the standard image  $B'$ , remove the black edge, and extract the effective image  $D'$ .

Step2: Perform 2D-LPEWT on image  $D'$ , and divide the transformed image low-frequency subband  $E'$  into non-overlapping sub-blocks of size  $8 \times 8$ , denoted as  $E'_{i,j}(i, j = 1, 2, \dots, M/8)$ .

Step3: Matrix Schur decomposition for each subblock.

$$[Q'_{i,j}, S'_{i,j}] = schur(E'_{i,j}) \quad (12)$$

$Q'_{i,j}$  is the unitary matrix decomposed by each sub-block  $E'_{i,j}$ , and  $S'_{i,j}$  is the upper triangular matrix.

Step4: Take the maximum value of each sub-block  $E'_{i,j}$  and denote it as  $E'_{(i,j)max}$ , and use  $E'_{(i,j)max}$  to construct a transition feature matrix  $F'$  of size  $(M/8) \times (M/8)$ , that is,

$$F'_{(i,j)} = E'_{(i,j)max}, \text{ where } (i, j = 1, 2, \dots, M/8), \text{ and calculate the sum}$$

of the elements in the transition matrix  $F'$  to obtain the mean value and denote it as  $F'_{mean}$ .

Step5: Generate a binary feature matrix, compare each element in the transition matrix  $F'$  with its mean  $F'_{mean}$  by formula(13), and obtain  $I'_{i,j}$ .

$$[Q'_{i,j}, S'_{i,j}] = schur(E'_{i,j}) \quad (13)$$

Step6: The detection image is obtained by XOR to generate a binary feature matrix  $I'$  and the zero-watermarking  $Z$  constructed before, and the scrambled binary watermark  $W^{*r}$  is obtained. Calculate the inverse Arnold transform of  $W^{*r}$  to obtain the watermark image  $W^*$  to be verified. The specific transformation formula is shown in formula (14):

$$W^{*r} = I' \oplus Z \quad (14)$$

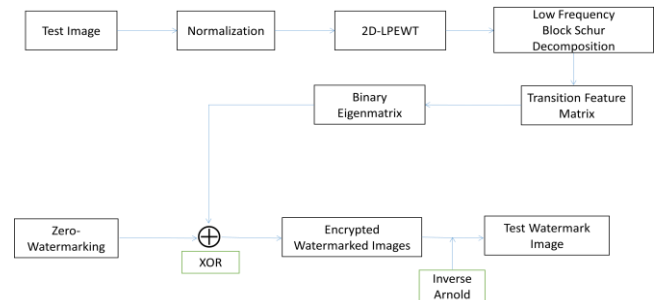


Fig. 5. Zero-watermarking extraction algorithm

## 4. Robustness experimental

### 4.1 Experimental platform and parameter description

The experiments of this subject are carried out on the Windows 10 operating system and the MATLAB R2014a platform. The original image is from the CVG-UGR image library, and the image size is  $512 \times 512$ . For binary copyright image, the words "LLMZ" with size  $64 \times 64$  are selected as shown in Figure 6. The scrambling number  $n = 8$  of the Arnold transform.



Fig. 6. Binary copyright image

The robustness evaluation standard of the zero-watermarking algorithm adopts the Normalized Correlation (NC). The size of the NC value represents the similarity between the original watermark and the watermark of the attacked image, and the larger the NC value, the higher the similarity of the images. The specific calculation formula of NC value is shown in formula (15):

$$NC = \frac{\sum_{i=1}^m \sum_{j=1}^n W(i, j)W'(i, j)}{\sqrt{\sum_{i=1}^m \sum_{j=1}^n [W(i, j)]^2} \sqrt{\sum_{i=1}^m \sum_{j=1}^n [W'(i, j)]^2}} \quad (15)$$

$W$ ,  $W'$  represent the original watermark and the extracted watermark.  $NC \in [0,1]$ . When  $NC=1$ , it means that the two watermarked images are identical, and when  $NC=0$ , it means that the two watermarks are not related.

4.2 False alarm rate testing and analysis

The images Barbara, Baboon, Plane, Lena and Goldhill are selected for test analysis.



Fig. 7. Test image

The specific results are shown in Table 1. It can be seen from the running results that the maximum value between the generated zero-watermarking signals is 0.6838, so it can be concluded that the zero-watermarking signals generated by the algorithm in different carrier images are related to the content of the image itself. The performance is higher, the false alarm rate is lower, and the algorithm is more secure.

Tab. 1. False alarm rate test table.

	Barbara	Baboon	Plane	Lena	Goldhill
Barbara	1.0000	0.5545	0.6838	0.6766	0.5125
Baboon	0.5545	1.0000	0.2243	0.5441	0.5563
Plane	0.6838	0.2243	1.0000	0.6637	0.6529
Lena	0.6766	0.5411	0.6637	1.0000	0.6035
Goldhill	0.5125	0.5563	0.6529	0.6035	1.0000

4.3 Robustness testing and analysis

Noise attack test

The Gaussian noise density is {0.01, 0.05, 0.1, 0.5}, the salt and pepper noise density is {0.01, 0.05, 0.1, 0.5}, and the multiplicative noise density is {0.01, 0.05, 0.1, 0.5}. The experimental data in the table shows that as the noise density increases, the NC value for watermark extraction decreases. The test images were attacked with Gaussian noise, salt and pepper noise and multiplicative noise of different intensities. When the noise intensity was less than or equal to 0.1, the NC value of the watermark was greater than 0.98, and when the noise intensity was 0.5, the NC value was greater than 0.95. The results show that the algorithm can resist different types and intensities of noise attacks.

Tab. 2. Noise attack NC value table

Attack	Parameter	Barbara	Baboon	Plane	Lena	Goldhill
Salt and Pepper	0.01	0.9992	0.9985	0.9992	0.9992	0.9977
	0.05	0.9974	0.9977	0.9951	0.9981	0.9966
Noise	0.1	0.9955	0.9936	0.9925	0.9977	0.9917
	0.5	0.9860	0.9751	0.9856	0.9906	0.9891

Gaussian	0.01	0.9970	0.9977	0.9953	0.9985	0.9985
	0.05	0.9932	0.9947	0.9923	0.9951	0.9925
	0.1	0.9928	0.9921	0.9909	0.9921	0.9909
Multipliative	0.5	0.9849	0.9811	0.9769	0.9879	0.9849
	0.01	0.9998	0.9992	0.9992	0.9989	0.9974
	0.05	0.9989	0.9943	0.9849	0.9932	0.9943
Noise	0.1	0.9940	0.9932	0.9825	0.9928	0.9936
	0.5	0.9803	0.9626	0.9569	0.9837	0.9724

Filter attack test

The original images were tested by three types of filtering attack: median filter, Gaussian filter and mean filter. Median filtering replaces the original pixel values of the image with the median value of the window size. Gaussian filtering is used as a smoothing filter to remove high frequency information in the image. Mean filtering refers to replacing the original pixel values of an image with the average value of the window size. The NC values are shown in Table 3: the overall NC values are above 0.98 for different filtering attacks, which indicates that the algorithm has strong resistance to different filtering attacks.

Tab. 3. Filtering attack NC value table

Attack	Parameter	Barbara	Baboon	Plane	Lena	Goldhill
Median Filter	3×3	0.9989	0.9970	0.9981	0.9989	0.9913
	5×5	0.9959	0.9957	0.9955	0.9989	0.9925
	7×7	0.9921	0.9914	0.9898	0.9985	0.9940
Gaussian	3×3	0.9974	0.9926	0.9966	0.9974	0.9983
	5×5	0.9966	0.9864	0.9962	0.9985	0.9940
	7×7	0.9966	0.9856	0.9962	0.9966	0.9940
Mean	3×3	0.9966	0.9871	0.9966	0.9977	0.9942
	5×5	0.9940	0.9856	0.9911	0.9955	0.9951
	7×7	0.9917	0.9834	0.9841	0.9940	0.9845

JPEG compression attack test

As the current international compression standard, JPEG compression is widely used in the field of digital watermarking. High-intensity JPEG compression attacks have a greater impact on image quality. The original images tested were subjected to JPEG compression attacks of different intensities, and the experimental results are shown in Table 4. When the compression is 10% of the image, the NC value remains above 0.99. For high-intensity compression 1% attack, the NC values are all above 0.97. The experimental results show that the algorithm has strong robustness to JPEG compression of different strengths.

Tab. 4. JPEG compression attack NC value table.

Attack	Parameter	Barbara	Baboon	Plane	Lena	Goldhill
JPEG	70	1.0000	0.9996	1.0000	0.9992	0.9998
	50	1.0000	0.9996	1.0000	1.0000	0.9996
	30	1.0000	1.0000	0.9996	0.9996	0.9951
	10	0.9943	0.9925	0.9931	0.9989	0.9981
	1	0.9917	0.9913	0.9714	0.9796	0.9834

Rotation Attack Test

In order to test the ability of the algorithm to resist geometric attacks, counterclockwise rotation attacks with rotation angles of 1°, 30°, 60°, and 90° are performed on the original image tested. The experimental results show that the NC value can be kept above 0.98, and the algorithm proposed in this subject has strong robustness to rotation attacks.

Tab. 5. Rotation attack NC value table.

Attack	Parameter	Barbara	Baboon	Plane	Lena	Goldhill
Rotation	1°	0.9962	0.9943	0.9955	0.9962	0.9925
	30°	0.9992	0.9868	0.9928	0.9917	0.9917
	60°	0.9985	0.9974	0.9940	0.9992	0.9981
	90°	0.9992	0.9940	1.0000	1.0000	0.9962

Scaling Attack Test

The scaling attack in this paper refers to scaling the original image tested by a certain proportion. The original images tested were attacked with scaling ratios of 0.5, 0.75, 1.5, and 2, respectively. It can be seen from Table 6 that the NC values of the watermarks are all greater than 0.9980, indicating that the algorithm has a good ability to resist image scaling attacks.

Tab. 6. Scaling attack NC value table.

Attack	Parameter	Barbara	Baboon	Plane	Lena	Goldhill
Scaling	0.5	0.9938	0.9981	0.9879	0.9951	0.9923
	0.75	0.9977	0.9955	0.9879	0.9985	0.9921
	1.5	0.9977	0.9974	1.0000	0.9913	0.9962
	2	0.9940	0.9974	1.0000	0.9996	0.9981

Translation Attack Test

In order to test the ability of the algorithm to resist translation attacks, the original image tested is shifted up by 20, 50 rows, and shifted to the left by 20, 50 columns. The experimental results are shown in Table 8. It is not difficult to see that the NC values of the watermarks are all greater than 0.9990, indicating that the algorithm has a good ability to resist image translation attacks.

Tab. 7. Translation attack NC value table.

Attack	Parameter	Barbara	Baboon	Plane	Lena	Goldhill
Translation	up 20	1.0000	1.0000	1.0000	1.0000	0.9974
	up 50	0.9985	0.9977	1.0000	1.0000	0.9947
	left 20	1.0000	1.0000	0.9975	0.9959	1.0000
	left 50	1.0000	1.0000	1.0000	0.9917	1.0000

4.4 Robustness comparative experimental analysis

This subject uses the Lena image in the image library as the carrier image, and carries out various intensities of attacks, and compares it with the similar methods of generating zero-watermarking. The comparison results are shown in Table 8: The zero-watermarking algorithm based on integer wavelet transform is selected CENG et al., based on the discrete wavelet transform Schur decomposition of the zero-watermarking algorithm LIU et al. for comparison. The comparative experimental results

show that for general non-geometric attacks and geometric attacks, the robustness of the algorithm proposed in this paper is higher than that of the zero-watermarking algorithm based on wavelet transform proposed in the other two literatures.

Tab. 8. Comparative experiment analysis NC value table.

Attack	Parameter	CENG et al.	LIU et al.	Proposed
Gaussian	0.05	0.9800	0.9866	0.9985
	0.1	0.9722	0.9827	0.9976
Noise	0.5	0.9048	0.9508	0.9890
	0.05	0.9838	0.9939	0.9981
Salt and Pepper	0.1	0.9561	0.9885	0.9977
	0.5	0.8467	0.9559	0.9906
Median Filter	3×3	0.9971	0.9987	0.9989
	5×5	0.9922	—	0.9981
Gaussian Filter	3×3	0.9949	0.9968	0.9974
	5×5	0.9951	0.9955	0.9985
JPEG	10	0.9895	0.9949	0.9989
	1	—	0.9763	0.9796
Rotation	1°	0.9380	0.9702	0.9962
	-1°	—	0.9749	0.9962

5. Summary

In this paper, we propose a robust zero-watermarking algorithm based on image moment normalization and 2D-LPEWT-Schur decomposition. The image translation, rotation and scaling invariance are achieved by normalization, the low-frequency subbands of the image are extracted by 2D-LPEWT, and the feature matrix is generated by block Schur decomposition, and finally the encrypted copyright image is XOR to generate zero-watermarking. The algorithm is robust to geometric and non-geometric attacks. Compared with CENG et al. and LIU et al., our proposed new zero-watermarking algorithm is more robust to rotation attack, noise attack, filtering attack, JPEG compression attack and scaling attack. And the proposed new zero-watermarking algorithm also has great potential in zero-watermarking construction of medical images.

Acknowledgements

This work was supported by The National Natural Science Foundation of China (No.61702184).

References

Wen Q, SUN T, Wang S. Concept and application of zero-watermark[J]. ACTA ELECTRONICA SINICA, 2003, 31(2): 214.

Shobana P, Kannan D. An Efficient Digital Rights Management Technique Based on Singular Value Decomposition[J]. Biometrics and Bioinformatics, 2011, 3(9): 424-428.

Prathap I, Natarajan V, Anitha R. Hybrid robust watermarking for color images[J]. Computers & Electrical Engineering, 2014, 40(3): 920-930.

Waleed J, Jun H D, Hameed S. A robust optimal zero-watermarking technique for secret watermark sharing[J]. International Journal of Security and Its Applications, 2014, 8(5): 349-360.

Yang K, Wang W, Yuan Z, et al. Strong robust zero watermarking algorithm based on NSCT transform and image normalization[C]//2018 IEEE 3rd Advanced Information Technology, Electronic and Automation Control Conference (IAEAC). IEEE, 2018: 236-240.

Gao G, Jiang G. Bessel-Fourier moment-based robust image zero-watermarking[J]. Multimedia Tools and Applications, 2015, 74(3): 841-858.

- Min L, Ting L, Yu-jie H. Arnold transform based image scrambling method[C]/3rd International Conference on Multimedia Technology (ICMT-13). Atlantis Press, 2013: 1302-1309.
- Huang N E, Shen Z, Long S R, et al. The empirical mode decomposition and the Hilbert spectrum for nonlinear and non-stationary time series analysis[J]. Proceedings of the Royal Society of London. Series A: mathematical, physical and engineering sciences, 1998, 454(1971): 903-995.
- Gilles J. Empirical wavelet transform[J]. IEEE transactions on signal processing, 2013, 61(16): 3999-4010.
- Gilles J, Tran G, Osher S. 2D empirical transforms. Wavelets, ridgelets, and curvelets revisited[J]. SIAM Journal on Imaging Sciences, 2014, 7(1):157-186.
- Current topics in microbiology and immunology[M]. Springer Berlin Heidelberg, 1974.
- Averbuch A, Coifman R R, Donoho D L, et al. Fast and accurate polar Fourier transform[J]. Applied and computational harmonic analysis, 2006, 21(2):145-167.
- Averbuch A, Coifman R R, Donoho D L, et al. A framework for discrete integral transformations I—the pseudopolar Fourier transform[J]. SIAM Journal on Scientific Computing, 2008, 30(2):764-784.
- Li Z, Zhou W, Chang Y, et al. A noise reduction method based on EWT-ICA for spectrum induced polarisation data[J]. Exploration Geophysics, 2021, 52(2):170-178.
- XIA Feng, LU Caiwu, GU Qinghua. Research on 2D empirical wavelet transform noise reduction of UAV stope images [J]. Science of Surveying and Mapping, 2021, 46(1): 108-113.
- Jin X, Jiang Q, Chu X, et al. Brain medical image fusion using l2-norm-based features and fuzzy-weighted measurements in 2-D Littlewood–Paley EWT domain[J]. IEEE Transactions on Instrumentation and Measurement, 2019, 69(8):5900-5913.
- GONG Rui, WANG Xiaochun. Multi-focus image fusion method based on C-EWT. Computer Engineering and Applications, 2020, 56(2): 201-210
- Keivani M, Sazdar A M, Mazloun J, et al. Application of Empirical Wavelet Transform in Digital Image Watermarking[J]. Traitement du Signal, 2020, 37(5).
- CHEN Hongsong, MENG Caixia, LIU Shuyu. Privacy Protection Experimental Research on Genes Association[J]. Journal of Hunan University(Natural Sciences) , 2020, 47(02):125-133.
- Mohammad A A. A new digital image watermarking scheme based on Schur decomposition[J]. Multimedia Tools and Applications, 2012, 59(3):851-883.
- Bing H. Zero color image watermarking based on Radon transform and quaternion real matrix[J]. Optical Technique, 2016: 166-171.
- Dong P, Brankov J G, Galatsanos N P, et al. Digital watermarking robust to geometric distortions[J]. IEEE Transactions on Image Processing, 2005, 14(12):2140-2150.
- CENG Wen-quan, XIONG Xiang-guang. Robust Zero Watermarking Algorithm Based on Integer Wavelet Transform[J]. Microelectronics & Computer, 2016, 33(4): 97-101, 107.
- LIU Wanjun, SUN Siyu, QU Haicheng. Fast Zero-Watermarking Algorithm Based on Schur Decomposition[J]. Journal of Frontiers of Computer Science and Technology, 2019, 13(3): 494-504.



**Lymuzhi Li** He was born in Wen Zhou, Zhejiang province, China in 1996. Now, he is a graduate student of Graduate School of North China University of science and technology, studying in cyberspace security, mainly researches on zero-watermarking and blockchain.



**Kunjie Cai** He was born in Mao Ming, Guangdong province, China in 1995. Now, he is a graduate student of Graduate School of North China University of science and technology, studying in cyberspace security, mainly researches on repackaged Android apps detection.



**Shuai Li** He was born in Han Dan, HeBei province, China in 1998. Now, he is a graduate student of Graduate School of North China University of science and technology, studying in network and information security, mainly researches on data security and privacy protection..



**Jincui Chang** received his B.Sc. degree in 1996 from Ocean University of China, received his M.Sc. degree in 2005 from Yanshan University, received his Ph.D. degree in 2008 from Dalian University of technology, now he is Professor in North China University of Science and technology. His main research interests include theories and methods in mathematical modelling and scientific computation, numerical

approximation and computational geometry, etc.